BNL-211750-2019-JAAM

Thermodynamics of Dual Doping in Quantum Dots

M. Makkar, S. Khalid

To be published in "Journal of Physical Chemistry Letters"

April 2019

Photon Sciences

Brookhaven National Laboratory

U.S. Department of Energy

USDOE Office of Science (SC), Basic Energy Sciences (BES) (SC-22)

DISCLAIMER

Thermodynamics of Dual Doping in Quantum Dots

Mahima Makkar,[†] Avijit Saha,[†] Syed Khalid,[§] and Ranjani Viswanatha*[,†,‡]

[†]New Chemistry Unit and [‡]International Centre for Materials Science, Jawaharlal Nehru Centre for Advanced Scientific Research, Jakkur, Bangalore 560064, India

[§]Brookhaven National Laboratory, Upton, New York 11973-5000, United States

ABSTRACT: Dual doping is a powerful way to tailor the properties of semiconductor quantum dots (QDs) arising out of host−dopant and dopant−dopant interactions. Nevertheless, it has seldom been explored due to a variety of thermodynamic challenges, such as the differential bonding strength and diffusion constant within the host matrix that integrates with the host in dissimilar ways. This work discusses the challenges involved in administering them within the constraints of one host under similar conditions of temperature, time, and chemical parameters such as solubility and reactivity using CoPt-doped CdS QDs as a model system. In addition, the various forces in play, such as Kirkendall diffusion, solid- and liquid-state diffusion, interaction of the hard acid soft base with the host, and the effect of lattice strain due to lattice mismatch, are studied to understand the feasibility of the core to doped transformation. These findings suggest a potential approach for manipulating the properties of semiconductors by dual doping engineering.

Doping in semiconductor quantum dots (QDs) has emerged as a technologically important tool for inducing properties that are otherwise not present in the host. It produces intriguing properties that arise from new electronic states created by optically active dopants[1−3] resulting in different emissions,[4−9] magnetic properties induced in non-magnetic hosts through magnetic dopants,[10−13] and surface plasmon resonance as a result of altering the charge carrier density in semiconductor QDs.[14−16] These properties have been instrumental for various applications in the fields of optoelectronics,[17] photovoltaics,[18,19] photodetectors,[20−22] light-emitting diodes,[23−25] and spin photonics. In particular, along with the dopant-induced properties, dual-doped QDs are expected to yield synergistic properties that are not observed in either of the individually doped systems. These properties include the change in the electrical properties arising from aliovalent doping.[26] The optical properties of a long-lived dopant emission can be influenced by another short-lived dopant emission and can provide extensive information about the spin dynamics of the long-lived emission from a fundamental perspective.[27] This, in turn, can be used to control the optical properties of a material by modulating the spin of the materials. Similarly, magnetic properties are also modulated by the presence of more than one dopant ion;[12] for example, the presence of a nonmagnetic spacer like Pt in the presence of either Fe or Co enhances its magnetism. Hence, it is important to be able to obtain uniformly doped QDs with more than one dopant ion.

The most challenging bottleneck in the development of these materials remains in the chemistry behind designing such materials with control over size, dopant distribution, and doping percentage where reproducibility remains difficult. This enormous challenge can be traced back to the stabilization of the metastable states overcoming the basic thermodynamically driven properties such as clustering of dopants, phase segregation, surface doping, and self-purification.[28−30] It is important to note that while dopant-induced changes in the properties of materials have been well studied, the concept of doping and the thermodynamic challenges in the design of different doped nanostructures have rarely been investigated. One of the recently developed methods demonstrates the constructive use of self-purification to obtain a uniform distribution of dopants within the host in a controlled manner.[31] The corresponding study of thermodynamics for the efficient use of this method yielded a few parameters that are responsible for effective doping, namely, the bond strength of the core and the diffusion constant of dopants in the host matrix.[7] However, dual doping of QDs has not yet been studied from a thermodynamic perspective. Additional challenges of dual doping include the differential bonding strength, the diffusion kinetics of the two different dopants that are not necessarily similar, and their differential substitution into the lattice, and hence, they pose additional problems for attaining uniform doping.

The various methods used to achieve doping include remote doping or modulation doping,[26,32,33] cation exchange,[34] surface doping, ligand modulation and other postdeposition techniques,[35] and QD superlattice doping.[36] However, most of these techniques try to overcome the energetic barrier to achieve a metastable equilibrium and hence are nontrivial for achieving a

Scheme 1. Diffusion of Binary Alloys into a Solid Matrix Due to the Kirkendall Effect and Increased Lattice Strain

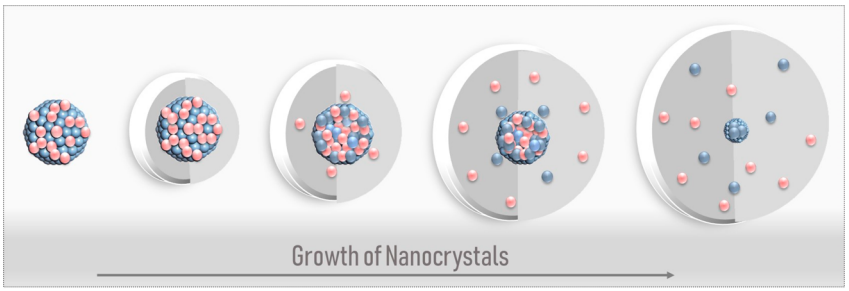

high level of success across various systems. Recently, diffusion doping from within the core to the outside has been discussed because of its relative ease and success across various dopants.[7] In this work, we study the various thermodynamic challenges specific to more than one impurity doping of nanocrystals using CoPt/CdS as the model system, including the Kirkendall effect, transient lattice strain due to the lattice mismatch between the core and shell, and hard soft acid base (HSAB) theory.

Herein, we demonstrate the use of the Kirkendall effect to trigger the diffusion for the effective distribution of dual dopants in QDs. While the Kirkendall effect, which is basically the motion of the interface between two metals that occurs as a consequence of the difference in the diffusion rates of the metal atoms, has been used to obtain dopant-induced hollow nanostructures,[37−39] its use to obtain uniformly doped QDs in this report is the first of its kind. Though the short bond length and high bond dissociation energy of the CoPt alloy make it a very sturdy material for various catalytic reactions,[40] this very same property hinders the diffusion of CoPt ions into the CdS matrix. For effective doping of Co and Pt into the host matrix, the first step is to overcome the lattice energy of the core. In this work, we increase the lattice strain due to the lattice mismatch at the interface with successive overcoating. This increase in transient stress during the shell growth is responsible for weakening the CoPt alloy core leading to diffusion of ions. We then use the differential diffusion coefficients of the components in an interdiffusion zone, also known as the Kirkendall effect, to trigger doping of CoPt in the CdS matrix. The lattice strain generated during overcoating of CoPt followed by the differential diffusion of the dopants due to the Kirkendall effect results in preferential diffusion of one element over the other. This preferential diffusion is studied using high-angle annular dark field energy-dispersive X-ray spectroscopy (HAADF-EDS) mapping, extended X-ray absorption fine structure (EXAFS), and inductively coupled plasma optical emission spectroscopy (ICP-OES). It should be noted that even though energy-dispersive X-ray spectroscopy in a scanning transmission electron microscope (STEM-EDS) would give the most direct mapping, within the resolution of interest for the optical and magnetic properties, that is the cluster of two or three atoms, it would not be able to be resolved within the constraints of this technique. However, this technique is useful for understanding the overall diffusion of Pt within the QD. EXAFS, on the other hand, is a slightly indirect way, but because of its sensitivity to the local structure at the atomic level, EXAFS can provide the exact information about the coordination environment.[41] Once the lattice is broken, similar to the single-dopant case, self-purification[42−44] also assists in the process of diffusion, which is not discussed herein. In this work, we have focused on equilibrium thermodynamics, via the systematic study of the transfer of matter and energy in systems as they pass from one state of a thermodynamic equilibrium to another. We have addressed the transformation of a stable core to a completely doped system, and the influence of thermodynamic parameters such as temperature and heat (annealing), energy (in the form of lattice strain), and work (diffusion of a stable core into the host matrix) has been studied. Also, the effect of HSAB theory on the efficiency of the bonding of the dopants in substitutional sites has been studied. We use X-ray diffraction (XRD), STEM-EDS, and EXAFS at various stages of material synthesis to understand the process of doping. We then demonstrate the consequent magnetic properties of the dopant clustered and the dopant uniformly distributed within the CdS matrix to study the effect of clustering of magnetic impurities on its properties.

CoPt core QDs were synthesized using colloidal methods (see the Supporting Information) with a uniform size distribution as observed in the transmission electron microscopy (TEM) image (6.6 ± 0.56 nm) shown in Figure S1a. The high-quality crystalline nature of these QDs is evident from the high-resolution TEM (HRTEM) image shown in the inset of Figure S1a. The XRD pattern for the bimetallic CoPt QDs along with the bulk data obtained from the inorganic crystal structure database (ICSD) is shown in Figure S1b with clear evidence of the formation of cubic CoPt QDs. The core CoPt QDs were then overcoated with a thick layer of CdS using the modified successive ionic layer adsorption and reaction (SILAR) method[45] to obtain a core−shell system. Here, the average particle size for the QDs is 10.9 ± 1.04 nm, and the magnetic ion percentage is found to be 5.8% as obtained by ICP-OES. Various properties of this clustered CoPt/CdS with a core of CoPt and a shell of CdS have been extensively studied.[46,47] The high bond strength of the CoPt alloy is responsible for a rather sharp interface between the clustered CoPt core and the CdS shell.

In an effort to overcome this energy, we resort to Kirkendall diffusion along with the simultaneous increase in lattice strain as shown in Scheme 1. The Kirkendall effect is the motion of the boundary between two metals that is triggered by the widely differing diffusion constants of the two metals. In this specific case, high-temperature annealing initiates the diffusion of Co preferentially over Pt. Additionally, this process is further assisted by incrementally increasing the lattice strain by simultaneously overcoating further shells of CdS. In the following sections, we study the effect of solution route annealing with and without overcoating as well as solid-state annealing as a function of time to understand the effect of differential diffusion and lattice strain.

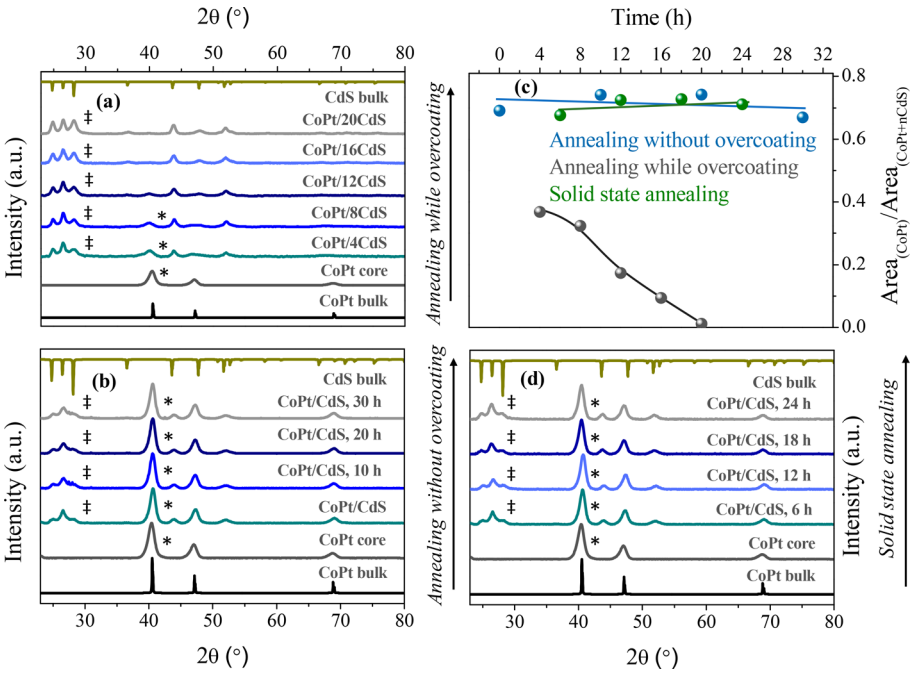

Figure 1. XRD patterns of CoPt/CdS QDs: (a) annealing while overcoating where the number corresponds to the number of shells, (b) annealing without overcoating of the core/shell system with a particular shell thickness, (c) ratio of the area of major XRD peaks of CoPt and CdS, and (d) solid-state annealing of the core/shell system with a particular shell thickness.

The first two parameters discussed herein include the presence of lattice strain as well as the state of the system. It is well-known that lattice mismatch leads to an increasing amount of lattice strain with an increasing thickness of the second material. In this work, we compare the XRD patterns in the presence and absence of overcoating during the annealing process to study the effect of an increase in lattice strain, and the results are plotted in panels a and b of Figure 1, respectively. XRD patterns of CoPt/CdS at different stages of diffusion along with bulk XRD for CoPt and CdS obtained from ICSD are shown in panels a and b of Figure 1. Diffusion of the dopants into the CdS lattice is quantified by considering the ratio of the area of major XRD peaks of CoPt (marked by an asterisk) and CdS (marked by a double dagger) as a function of time and is shown in Figure 1c. From the figures, it is evident that when the annealing at high temperatures is carried out along with overcoating of thicker layers of CdS (Figure 1a), the CoPt:CdS area ratio decreases, eventually exhibiting only the CdS feature with a complete absence of the CoPt feature. In contrast, annealing at high temperatures without simultaneous overcoating does not change the area ratio of these characteristic peaks, suggesting the absence of any diffusion of CoPt in these QDs as shown in Figure 1c. This suggests that the lattice strain created by continued overcoating of CdS is necessary to initiate the diffusion of CoPt into the CdS lattice. Second, even though solid-state diffusion is slower than that in the solution phase, it is unclear if diffusion can be triggered in the solid state. Hence, we study the diffusion of CoPt by annealing of the drop-casted film of the CoPt/CdS core/shell system as shown in Figure 1d in comparison to solution phase annealing. A similar study with the ratio of two peak areas as a function of annealing time in QD films is shown in Figure 1c, demonstrating the absence of diffusion in the solid state. Thus, in the absence of strain due to lattice mismatch created by subsequent overcoating, simple high-temperature annealing is not enough to result in diffusion of the CoPt lattice. Hence, it is necessary to anneal the QDs while overcoating in the solution phase. It is important to note here that it is essential to carefully balance the annealing time and temperature of growth such that the rate of diffusion of the magnetic Kirkendall core is slower than the rate of growth of the shell by the SILAR technique. This controlled diffusion allows us to have command of the percentage and uniformity of dual doping and the size of the QDs.

It should be noted that within the core/shell architecture, it is apparent that the magnetic ions are localized within a particular nanoscopic volume of the semiconductor surrounded by a nonmagnetic CdS matrix as shown in the TEM and HRTEM images in panels a and c of Figure 2, respectively. From the HRTEM image (Figure 2c), it is evident that the lattice planes in the core are different from that of the shell, suggesting a core/shell kind of structure as expected. Typical TEM and HRTEM images of these diffused CoPt/CdS are shown in panels b and d of Figure 2, respectively. The absence of contrast in the electron density (Figure 2b) unlike that of the core/shell demonstrates the absence of a metallic CoPt core. Moreover, the HRTEM image of the QDs, shown in Figure 2d, does not reveal any lattice mismatch or possible clustering of other materials, demonstrating the diffuse nature of Co and Pt in the host CdS lattice on the TEM scale. Similarly, the X-ray diffraction patterns shown in Figure 2e demonstrate the absence of CoPt lattice peaks in the diffused structure that is otherwise observed in clustered CoPt/CdS. To further confirm the distribution of the lattice, we carried out STEM-EDS mapping on the diffused CoPt/CdS, and the results are shown in Figure 2f–i. EDS mapping within the resolution range (~5 nm) shows a diffuse distribution of both dopants, Co (Figure 2h) and Pt (Figure 2i), within the selected area for the diffused CoPt/CdS structure. From a fundamental perspective, while it is evident from the XRD and TEM that the diffusion of CoPt into the CdS lattice has occurred, the mechanism of diffusion and the order of diffusion

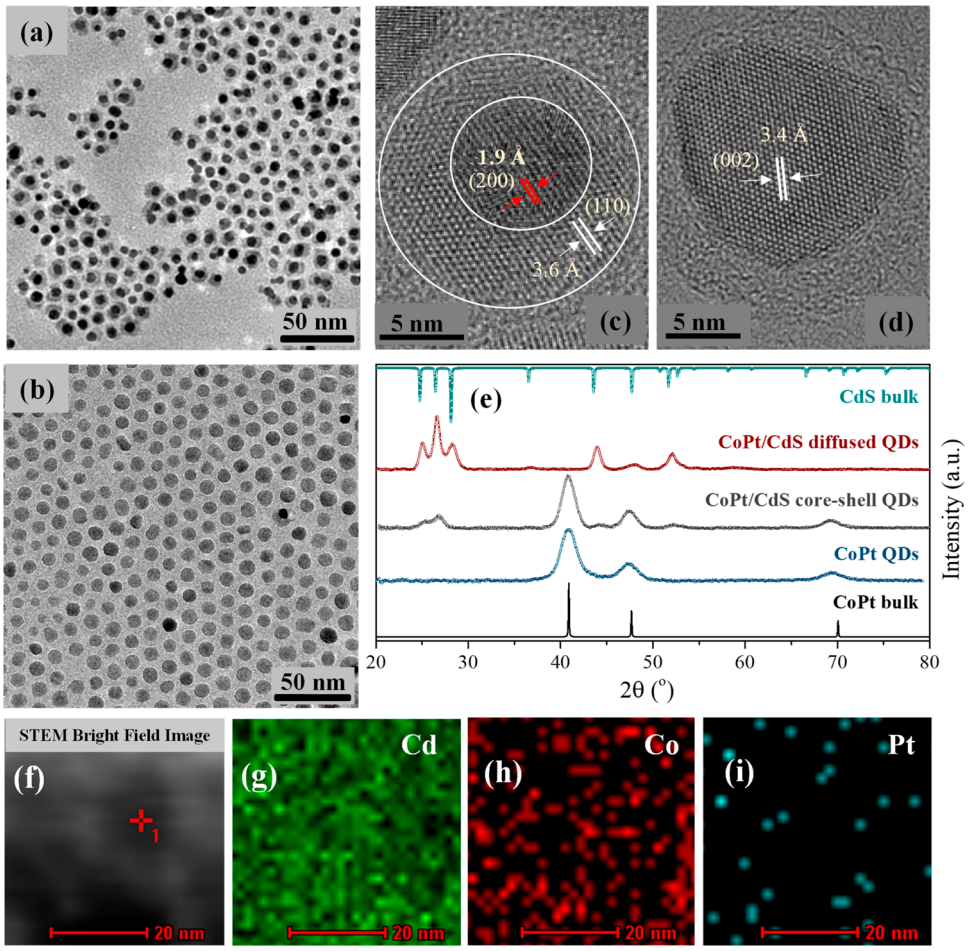

Figure 2. (a) TEM image showing CoPt/CdS core/shell QDs (11.3 ± 1.71 nm). (b) TEM image showing Co- and Pt-diffused CdS QDs (10.9 ± 1.04 nm). (c and d) Representative high-resolution TEM images. (e) XRD pattern of the CoPt/CdS core/shell QDs and Co- and Pt-diffused CdS QDs. STEM-EDS mapping of Co- and Pt-diffused CdS QDs showing the STEM (f) bright field image, (g) Cd map, (h) Co map, and (i) Pt map.

are unknown. For example, because Pt and Cd are considered softer than Co, by the HSAB principle,[48] one would expect Pt to replace Cd earlier than Co. However, it is well-known that the diffusion coefficient of Pt is lower than that of Co.[49] Hence, it is important to study the rate-determining step to understand the thermodynamically viable dual doping mechanism. Additionally, even though XRD, TEM, and EDS mapping show the absence of clustering in the diffused QDs, on the typical length scales of XRD and TEM, it is nontrivial to locate clusters of 3−10 magnetic ions within the vicinity that can be detrimental to their properties.

Hence, to study the local clustering and the doping mechanism, we measured the XAFS edges of both dopants for the core, core/shell, and diffused QD systems in fluorescence mode. EXAFS spectra were modeled to a theoretical model to generate relevant paths using FEFF6 within the ARTEMIS program.[50] Figure 3 shows the experimental data and the fit for core, core/shell, and diffused QDs for the Co K edge (Figure 3a−c, respectively) and the Pt L_3 edge (Figure 3d−f, respectively). Visual inspection of the data makes it evident that the local structure around Co and Pt has evolved within the QDs going from the core to the diffused QDs. In-depth analysis of the data using the proposed model suggests that the overcoating of CoPt with CdS under the synthesis conditions presented here brings about a change in the local environment of Co and Pt atoms. The presence of a high intensity at low R in Figure 3a suggests the presence of a Co−O layer on the surface of the core due to surface oxidation. In contrast, this oxidation is absent in the core/shell QDs as well as the diffused QDs. It is also interesting to note that this peak is either completely absent or minimal in the Pt environment, suggesting the presence of Co at the surface rather than Pt in the core confirming the Kirkendall diffusion leading to the formation of the CoO layer at the surface and voids with Pt clusters in the diffusion zone. The presence of excess Co at the surface as compared to Pt in the core is further confirmed by the ICP data as observed by the higher percentage of Co than of Pt, and these data are listed in Table S1. With an increase in the CdS shell thickness and high-temperature annealing, the contribution of the Co/S path is observed along with that of Co/Pt paths and minor contributions from other paths as shown in panels b and c of Figure 3 due to outward diffusion of Co ions into the host matrix. It is interesting to note that even though the Co/S path is quite prominent (Figure 3b) in the case of core/shell CoPt/CdS, the Pt/S path (Figure 3e) is minor due to the faster diffusion of Co compared to that of Pt. This leads to an increase in Pt/Pt coordination in the case of a core/shell system. However, in the case of diffused CdS QDs, we note an increase in the Pt/S contribution (Figure 3f), suggesting the successful diffusion of Pt into the CdS lattice, thus corroborating the XRD and TEM data. Various fitting

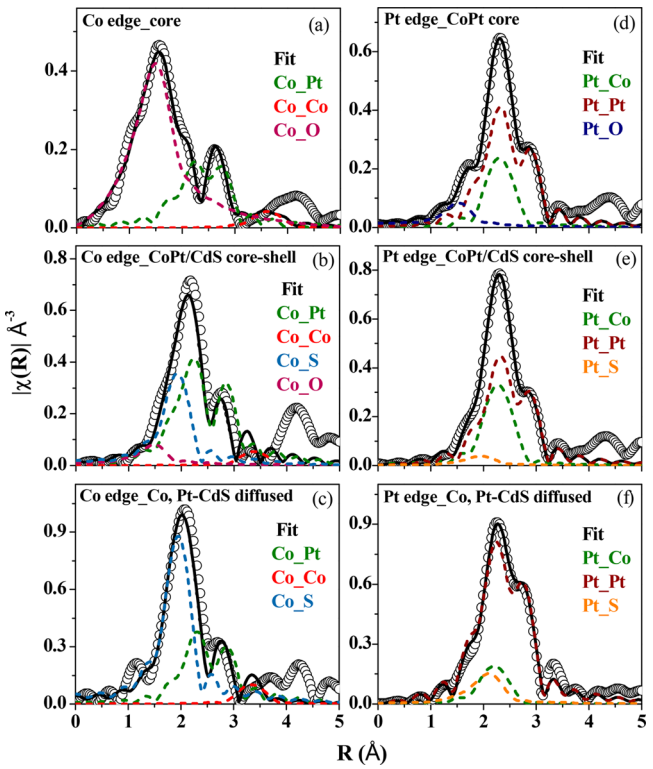

Figure 3. Magnitude of Fourier-transformed Co K edge and Pt L_3 edge EXAFS spectra (empty symbols) and their best fit (black line) for (a) the Co edge core, (b) Co edge core/shell, (c) Co edge diffused, (d) Pt edge core, (e) Pt edge core/shell, and (f) Pt edge diffused. Dashed lines show their component fitting paths.

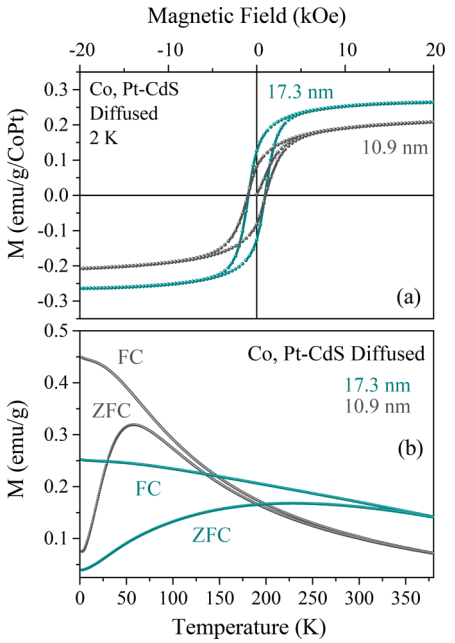

Figure 4. (a) Magnetization vs magnetic field for Co- and Pt-CdS diffused QDs of different sizes at 2 K. (b) FC and ZFC for Co- and Pt-CdS diffused QDs measured using a 200 Oe field.

parameters of the numerous paths used in fitting the data are listed in Table S2.

The final proof of the formation of cluster-free diffused dual-doped QDs is in its properties. The most compelling properties of the CoPt alloys are its optical and magnetic properties. Pt, as a diamagnetic spacer between the ferromagnetic Co dopants in CoPt/CdS, exhibits magnetic properties that are much better than those of Co-doped CdS with a coercivity of ∼1000 Oe and large saturation magnetization of 0.2 emu/g/CoPt at 2 K as shown in Figure S2. This is explained by the relativistic spin−orbit coupling effect of Pt wherein alloying of 3d elements with heavy 4d and 5d elements allows tuning of the magnetic anisotropic energy. This anisotropy in the system induces spin polarization of Pt atoms, although it is diamagnetic, followed by ferromagnetic coupling of Co and Pt atoms due to hybridization of Pt 5d and Co 3d states. The effect of the polarization of spins of Pt in the 5d band is utilized to obtain high-exchange interactions in CoPt/CdS QDs resulting in higher magnetization. Now it is interesting to study whether this synergistic effect of Pt on magnetic ordering can be extended to diffused QDs in which Co and Pt are at much larger distances and may or may not be ordered. The plots of magnetization versus applied field (M vs H) for diffused or doped QDs after correcting for the number of magnetic atoms and magnetization as a function of temperature (M vs T) are shown in panels a and b of Figure 4, respectively. The 10.9 nm diffused QDs show ∼0.2 emu/g/CoPt saturation magnetization at 2 K with a coercivity of ∼1000 Oe, which is much larger than the core/shell structure as shown in Figure S3. In addition, the FC and ZFC curves (Figure 4b) show that the 10.9 nm diffused QDs reach the blocked state below 57 K, which is comparable to or higher than that of core/shell QDs (Figure S3). We also synthesized larger diffused QDs (17.3 nm) as shown from the TEM image shown in Figure S4, and the plots of M versus H are shown in Figure 4a. As expected, we observe that the corresponding saturation magnetization is shown to scale with the size of the QDs consistent with the larger domain size. Similarly, the FC and ZFC measurements show that the larger particles remain in the blocked state up to 380 K as shown in Figure 4b, unlike the smaller ones that show a blocking temperature of only 57 K. From all of these data, it appears that these uniformly diffused QDs behave like complete magnetic grains and a large magnetic grain shows saturation magnetization that is higher than that of the smaller ones due to a significant change in domain size. Also, these diffuse Co- and Pt-doped CdS samples are optically active and exhibit strong absorption and emission. The absorption spectra show a peak corresponding to the band gap transition of CdS QDs in diffused CoPt/CdS, unlike the clustered CoPt/CdS QDs that are optically inactive with no band gap corresponding to the CdS QDs as shown in Figure S5. Steady-state PL spectra show a broad dopant emission peak due to Co doping at a higher wavelength along with the band edge emission at a lower wavelength.

Similar studies were performed on FePt/CdS QDs to prove the generality and universality of this technique. The basic characterization is shown in panels a and b of Figure S6, while the magnetic response of FePt/CdS QDs is shown in panels c and d of Figure S6. The diffused QDs show a saturation magnetization of ∼0.4 emu/g at 2 K. Measurements of M versus T of the QDs demonstrate the presence of a blocking temperature of 88 K. It is interesting to note that the diffusion of Fe, even though performed at a temperature (250 °C) higher than that of Co (220 °C), showed similar doping percentages upon annealing for identical periods of time. This suggests that the diffusion of Co in wurtzite CdS is faster than that of Fe.

In summary, we present experimental evidence that suggests that the Kirkendall effect and lattice strain can initiate the diffusion reactions of binary alloys into the II–VI semiconductor matrix. These parameters break ground for the systematic study of colloidal-state diffusion, and the results offer new insight into the microscopic mechanism of doping in colloidal QDs. We have demonstrated for the first time that the Kirkendall effect can be exploited for doping and can be extended to other Kirkendall pairs to result in a new class of dual-doped QDs.

XRD, TEM of CoPt core QDs, *M* versus *H* hysteresis and *M* versus *T* for CoPt/CdS core/shell QDs, ICP-OES data, XAFS fitting parameters, TEM, and *M* versus *H* hysteresis for different diffused QDs, absorption and photoluminescence spectra of core/shell and diffused QDs, XRD, TEM, *M* versus *H* hysteresis, and *M* versus *T* for FePt/CdS diffused QDs, and Experimental Section (PDF)

■ ACKNOWLEDGMENTS

The authors thank JNCASR, the Sheikh Saqr Laboratory, the Indian National Science Academy, and the Department of Science and Technology, Government of India, for financial support. XAFS was carried out at Stanford Synchrotron Radiation Lightsource, a U.S. Department of Energy (DOE) Office of Science User Facility operated for the DOE Office of Science by SLAC National Accelerator Laboratory under Contract DE-AC02-76SF00515. Use of SSRL BL2-2 was partially supported by National Synchrotron Light Source II, Brookhaven National Laboratory, under DOE Contract DE-SC0012704. EXAFS measurement at SSRL was supported by the Department of Science and Technology, Government of India (SR/NM/Z-07/2015), and the Jawaharlal Nehru Centre for Advanced Scientific Research (JNCASR) is thanked for managing the project. The authors thank Abhijit Sen for magnetic measurements and Kannan Dhandapani and Dr. Jay Ghatak for TEM imaging.

■ REFERENCES

(1) Grandhi, G. K.; Viswanatha, R. Tunable Infrared Phosphors using Cu Doping in Semiconductor Nanocrystals: Surface Electronic Structure Evaluation. *J. Phys. Chem. Lett.* **2013**, *4*, 409–415.

(2) Grandhi, G. K.; Swathi, K.; Narayan, K. S.; Viswanatha, R. Cu Doping in Ligand Free CdS Nanocrystals: Conductivity and Electronic Structure Study. *J. Phys. Chem. Lett.* **2014**, *5*, 2382–2389.

(3) Zhang, J.; Di, Q.; Liu, J.; Bai, B.; Liu, J.; Xu, M.; Liu, J. Heterovalent Doping in Colloidal Semiconductor Nanocrystals: Cation-Exchange-Enabled New Accesses to Tuning Dopant Luminescence and Electronic Impurities. *J. Phys. Chem. Lett.* **2017**, *8*, 4943–4953.

(4) Grandhi, G. K.; Tomar, R.; Viswanatha, R. Study of Surface and Bulk Electronic Structure of II–VI Semiconductor Nanocrystals Using Cu as a Nanosensor. *ACS Nano* **2012**, *6*, 9751–9763.

(5) Bhargava, R. N.; Gallagher, D.; Hong, X.; Nurmikko, A. Optical Properties of Manganese-Doped Nanocrystals of ZnS. *Phys. Rev. Lett.* **1994**, *72*, 416–419.

(6) Norris, D. J.; Yao, N.; Charnock, F. T.; Kennedy, T. A. High-Quality Manganese-Doped ZnSe Nanocrystals. *Nano Lett.* **2001**, *1*, 3–7.

(7) Saha, A.; Makkar, M.; Shetty, A.; Gahlot, K.; Pavan, A. R.; Viswanatha, R. Diffusion Doping in Quantum Dots: Bond Strength and Diffusivity. *Nanoscale* **2017**, *9*, 2806–2813.

(8) Grandhi, G. K.; M., A.; Viswanatha, R. Understanding the Role of Surface Capping Ligands in Passivating the Quantum Dots Using Copper Dopants as Internal Sensor. *J. Phys. Chem. C* **2016**, *120*, 19785–19795.

(9) Pradhan, N.; Sarma, D. Advances in Light-Emitting Doped Semiconductor Nanocrystals. *J. Phys. Chem. Lett.* **2011**, *2*, 2818–2826.

(10) Hanif, K. M.; Meulenberg, R. W.; Strouse, G. F. Magnetic Ordering in Doped $Cd_{1-x}Co_xSe$ Diluted Magnetic Quantum Dots. *J. Am. Chem. Soc.* **2002**, *124*, 11495–11502.

(11) Bonanni, A.; Dietl, T. A Story of High-Temperature Ferromagnetism in Semiconductors. *Chem. Soc. Rev.* **2010**, *39*, 528–539.

(12) Viswanatha, R.; Naveh, D.; Chelikowsky, J. R.; Kronik, L.; Sarma, D. D. Magnetic Properties of Fe/Cu Codoped ZnO Nanocrystals. *J. Phys. Chem. Lett.* **2012**, *3*, 2009–2014.

(13) Makkar, M.; Viswanath, R. Recent Advances in Magnetic Ion-Doped Semiconductor Quantum Dots. *Curr. Sci.* **2017**, *112*, 1421–1429.

(14) Garcia, G.; Buonsanti, R.; Runnerstrom, E. L.; Mendelsberg, R. J.; Llordes, A.; Anders, A.; Richardson, T. J.; Milliron, D. J. Dynamically Modulating the Surface Plasmon Resonance of Doped Semiconductor Nanocrystals. *Nano Lett.* **2011**, *11*, 4415–4420.

(15) Luther, J. M.; Jain, P. K.; Ewers, T.; Alivisatos, A. P. Localized Surface Plasmon Resonances Arising from Free Carriers in Doped Quantum Dots. *Nat. Mater.* **2011**, *10*, 361.

(16) Comin, A.; Manna, L. New Materials for Tunable Plasmonic Colloidal Nanocrystals. *Chem. Soc. Rev.* **2014**, *43*, 3957–3975.

(17) Choi, J. H.; Fafarman, A. T.; Oh, S. J.; Ko, D. K.; Kim, D. K.; Diroll, B. T.; Muramoto, S.; Gillen, J. G.; Murray, C. B.; Kagan, C. R. Bandlike Transport in Strongly Coupled and Doped Quantum Dot Solids: A Route to High-Performance Thin-Film Electronics. *Nano Lett.* **2012**, *12*, 2631–2638.

(18) Chuang, C.-H. M.; Brown, P. R.; Bulović, V.; Bawendi, M. G. Improved Performance and Stability in Quantum Dot Solar Cells Through Band Alignment Engineering. *Nat. Mater.* **2014**, *13*, 796–801.

(19) Carey, G. H.; Kramer, I. J.; Kanjanaboos, P.; Moreno-Bautista, G.; Voznyy, O.; Rollny, L.; Tang, J. A.; Hoogland, S.; Sargent, E. H. Electronically Active Impurities in Colloidal Quantum Dot Solids. *ACS Nano* **2014**, *8*, 11763–11769.

(20) Kufer, D.; Nikitskiy, I.; Lasanta, T.; Navickaite, G.; Koppens, F. H. L.; Konstantatos, G. Hybrid 2D–0D MoS_2–PbS Quantum Dot Photodetectors. *Adv. Mater.* **2015**, *27*, 176–180.

(21) Konstantatos, G.; Badioli, M.; Gaudreau, L.; Osmond, J.; Bernechea, M.; de Arquer, F. P. G.; Gatti, F.; Koppens, F. H. L. Hybrid Graphene–Quantum Dot Phototransistors With Ultrahigh Gain. *Nat. Nanotechnol.* **2012**, *7*, 363–368.

(22) Deng, Z.; Jeong, K. S.; Guyot Sionnest, P. Colloidal Quantum Dots Intraband Photodetectors. *ACS Nano* **2014**, *8*, 11707–11714.

(23) Sun, L.; Choi, J. J.; Stachnik, D.; Bartnik, A. C.; Hyun, B.-R.; Malliaras, G. G.; Hanrath, T.; Wise, F. W. Bright Infrared Quantum

Dot Light Emitting Diodes Through Inter-Dot Spacing Control. *Nat. Nanotechnol.* **2012**, *7*, 369−373.
(24) Yang, Y.; Zheng, Y.; Cao, W.; Titov, A.; Hyvonen, J.; Manders, J. R.; Xue, J.; Holloway, P. H.; Qian, L. High-Efficiency Light-Emitting Devices Based on Quantum Dots with Tailored Nanostructures. *Nat. Photonics* **2015**, *9*, 259−266.
(25) Saha, A.; Chellappan, K. V.; Narayan, K. S.; Ghatak, J.; Datta, R.; Viswanatha, R. Near-Unity Quantum Yield in Semiconducting Nanostructures: Structural Understanding Leading to Energy Efficient Applications. *J. Phys. Chem. Lett.* **2013**, *4*, 3544−3549.
(26) Kagan, C. R.; Murray, C. B. Charge Transport in Strongly Coupled Quantum Dot Solids. *Nat. Nanotechnol.* **2015**, *10*, 1013.
(27) Cao, S.; Li, C.; Wang, L.; Shang, M.; Wei, G.; Zheng, J.; Yang, W. Long-Lived and Well-Resolved Mn $^{2+}$ Ion Emissions in CuInS-ZnS Quantum Dots. *Sci. Rep.* **2015**, *4*, 7510.
(28) van Schilfgaarde, M.; Mryasov, O. N. Anomalous Exchange Interactions in III-V Dilute Magnetic Semiconductors. *Phys. Rev. B: Condens. Matter Mater. Phys.* **2001**, *63*, 233205.
(29) Sato, K.; Katayama -Yoshida, H.; Dederichs, P. H. High Curie Temperature and Nano-Scale Spinodal Decomposition Phase in Dilute Magnetic Semiconductors. *Jpn. J. Appl. Phys.* **2005**, *44*, L948−L951.
(30) Makkar, M.; Viswanatha, R. Frontier Challenges in Doping Quantum Dots: Synthesis and Characterization. *RSC Adv.* **2018**, *8*, 22103−22112.
(31) Saha, A.; Shetty, A.; Pavan, A. R.; Chattopadhyay, S.; Shibata, T.; Viswanatha, R. Uniform Doping in Quantum Dots Based Dilute Magnetic Semiconductor. *J. Phys. Chem. Lett.* **2016**, *7*, 2420−2428.
(32) Oh, S. J.; Kim, D. K.; Kagan, C. R. Remote Doping and Schottky Barrier Formation in Strongly Quantum Confined Single PbSe Nanowire Field-Effect Transistors. *ACS Nano* **2012**, *6*, 4328−4334.
(33) Luther, J. M.; Pietryga, J. M. Stoichiometry Control in Quantum Dots: A Viable Analog to Impurity Doping of Bulk Materials. *ACS Nano* **2013**, *7*, 1845−1849.
(34) Petralanda, U.; De Trizio, L.; Gariano, G.; Cingolani, R.; Manna, L.; Artyukhin, S. Triggering Cation Exchange Reactions by Doping. *J. Phys. Chem. Lett.* **2018**, *9*, 4895−4900.
(35) Engel, J. H.; Alivisatos, A. P. Postsynthetic Doping Control of Nanocrystal Thin Films: Balancing Space Charge to Improve Photovoltaic Efficiency. *Chem. Mater.* **2014**, *26*, 153−162.
(36) Cargnello, M.; Johnston Peck, A. C.; Diroll, B. T.; Wong, E.; Datta, B.; Damodhar, D.; Doan-Nguyen, V. V. T.; Herzing, A. A.; Kagan, C. R.; Murray, C. B. Substitutional Doping in Nanocrystal Superlattices. *Nature* **2015**, *524*, 450.
(37) Wang, W.; Dahl, M.; Yin, Y. Hollow Nanocrystals Through the Nanoscale Kirkendall Effect. *Chem. Mater.* **2013**, *25*, 1179−1189.
(38) Yin, Y.; Rioux, R. M.; Erdonmez, C. K.; Hughes, S.; Somorjai, G. A.; Alivisatos, A. P. Formation of Hollow Nanocrystals Through the Nanoscale Kirkendall Effect. *Science* **2004**, *304*, 711−714.
(39) Guria, A. K.; Prusty, G.; Patra, B. K.; Pradhan, N. Dopant-Controlled Selenization in Pd Nanocrystals: The Triggered Kirkendall Effect. *J. Am. Chem. Soc.* **2015**, *137*, 5123−5129.
(40) Guo, S.; Li, D.; Zhu, H.; Zhang, S.; Markovic, N. M.; Stamenkovic, V. R.; Sun, S. FePt and CoPt Nanowires as Efficient Catalysts for the Oxygen Reduction Reaction. *Angew. Chem.* **2013**, *125*, 3549−3552.
(41) Saha, A.; Chattopadhyay, S.; Shibata, T.; Viswanatha, R. Core−Shell to Doped Quantum Dots: Evolution of the Local Environment Using XAFS. *J. Phys. Chem. C* **2016**, *120*, 18945−18951.
(42) Erwin, S. C.; Zu, L.; Haftel, M. I.; Efros, A. L.; Kennedy, T. A.; Norris, D. J. Doping Semiconductor Nanocrystals. *Nature* **2005**, *436*, 91−94.
(43) Karan, N. S.; Sarkar, S.; Sarma, D. D.; Kundu, P.; Ravishankar, N.; Pradhan, N. Thermally Controlled Cyclic Insertion/Ejection of Dopant Ions and Reversible Zinc Blende/Wurtzite Phase Changes in ZnS Nanostructures. *J. Am. Chem. Soc.* **2011**, *133*, 1666−1669.
(44) Dalpian, G. M.; Chelikowsky, J. R. Self-Purification in Semiconductor Nanocrystals. *Phys. Rev. Lett.* **2006**, *96*, 226802.
(45) Li, J. J.; Wang, Y. A.; Guo, W.; Keay, J. C.; Mishima, T. D.; Johnson, M. B.; Peng, X. Large-Scale Synthesis of Nearly Monodisperse CdSe/CdS Core/Shell Nanocrystals Using Air-Stable Reagents Via Successive Ion Layer Adsorption and Reaction. *J. Am. Chem. Soc.* **2003**, *125*, 12567−12575.
(46) Gu, H.; Zheng, R.; Zhang, X.; Xu, B. Facile One-Pot Synthesis of Bifunctional Heterodimers of Nanoparticles: A Conjugate of Quantum Dot and Magnetic Nanoparticles. *J. Am. Chem. Soc.* **2004**, *126*, 5664−5665.
(47) Habas, S. E.; Yang, P.; Mokari, T. Selective Growth of Metal and Binary Metal Tips on CdS Nanorods. *J. Am. Chem. Soc.* **2008**, *130*, 3294−3295.
(48) Pearson, R. G. Hard and Soft Acids and Bases, HSAB, Part II: Underlying Theories. *J. Chem. Educ.* **1968**, *45*, 643.
(49) Xin, H. L.; Alayoglu, S.; Tao, R.; Genc, A.; Wang, C.-M.; Kovarik, L.; Stach, E. A.; Wang, L.-W.; Salmeron, M.; Somorjai, G. A.; Zheng, H. Revealing the Atomic Restructuring of Pt−Co Nanoparticles. *Nano Lett.* **2014**, *14*, 3203−3207.
(50) Ravel, B.; Newville, M. ATHENA and ARTEMIS: Interactive Graphical Data Analysis Using IFEFFIT. *Phys. Scr.* **2005**, *2005*, 1007.